



Universiteit
Leiden
The Netherlands

Canonical and non-canonical Wnt signaling in hematopoiesis and lymphocyte development

Famili, F.

Citation

Famili, F. (2018, May 30). *Canonical and non-canonical Wnt signaling in hematopoiesis and lymphocyte development*. Retrieved from <https://hdl.handle.net/1887/63077>

Version: Not Applicable (or Unknown)

License: [Licence agreement concerning inclusion of doctoral thesis in the Institutional Repository of the University of Leiden](#)

Downloaded from: <https://hdl.handle.net/1887/63077>

Note: To cite this publication please use the final published version (if applicable).

Cover Page



Universiteit Leiden



The following handle holds various files of this Leiden University dissertation:

<http://hdl.handle.net/1887/63077>

Author: Famili, F.

Title: Canonical and non-canonical Wnt signaling in hematopoiesis and lymphocyte development

Issue Date: 2018-05-30

CHAPTER 2

HIGH LEVELS OF CANONICAL WNT SIGNALING LEAD TO LOSS OF STEMNESS AND INCREASED DIFFERENTIATION IN HEMATOPOIETIC STEM CELLS

Farbod Famili,¹ Martijn H. Brugman,¹ Erdogan Taskesen,² Brigitta E.A. Naber,¹ Riccardo Fodde,³ and Frank J.T. Staal¹

¹*Department of Immunohematology and Blood Transfusion, Leiden University Medical Center, 2300 Leiden, the Netherlands*

²*Department of Clinical Genetics, VU University, 1081 Amsterdam, the Netherlands*

³*Department of Pathology, Erasmus Medical Center, 3000 Rotterdam, the Netherlands*

Stem Cell Reports j Vol. 6 j 652–659 j May 10, 2016

Summary

Canonical Wnt signaling regulates the self-renewal of most if not all stem cell systems. In the blood system, the role of Wnt signaling has been the subject of much debate but there is consensus that high Wnt signals lead to loss of reconstituting capacity. To better understand this phenomenon, we have taken advantage of a series of hypomorphic mutant *Apc* alleles resulting in a broad range of Wnt dosages in hematopoietic stem cells (HSCs) and performed whole-genome gene expression analyses. Gene expression profiling and functional studies show that HSCs with APC mutations lead to high Wnt levels, enhanced differentiation, and diminished proliferation but have no effect on apoptosis, collectively leading to loss of stemness. Thus, we provide mechanistic insight into the role of APC mutations and Wnt signaling in HSC biology. As Wnt signals are explored in various in vivo and ex vivo expansion protocols for HSCs, our findings also have clinical ramifications.

Introduction

In many tissues, including the blood, intestine and skin, old cells are eliminated and replenished by newly developed cells from a small pool of stem cells. This rare population of stem cells is located in a specific microenvironment, the niche, and gives rise to several different lineages of abundant daughter cells (Mendez-Ferrer et al., 2010). The signals controlling the various stem cell fates (self-renewal, differentiation, quiescence, apoptosis, and others) are beginning to be elucidated. A number of evolutionary conserved pathways are important for the development and maintenance of adult stem cells, including Notch, bone morphogenic protein, hedgehog, fibroblast growth factor, transforming growth factor- β , and Wnt signals (Blank et al., 2008). Among these pathways, the Wnt pathway is seen as a dominant factor in self-renewal of many types of adult stem cells (Reya and Clevers, 2005). Compared with the convincing studies on the role of Wnt signaling in adult stem cells in skin and gut, a role for Wnt in adult hematopoietic stem cells (HSCs) has proved much more difficult to demonstrate (reviewed in Luis et al., 2012). In studies reporting an important role for Wnt signaling in blood cells, Wnt seemed to be required for normal HSC self-renewal and therefore for efficient reconstitution after transplantation (Luis et al., 2011).

Several types of Wnt signaling can be discerned often referred to as the canonical or Wnt/ β -catenin pathway and the non-canonical pathways (reviewed extensively in Staal et al., 2008). In the absence of Wnt ligands, cytoplasmic levels of β -catenin are kept very low through the action of a protein complex (the so-called destruction complex) that actively targets β -catenin for degradation. This complex is composed of two negative regulatory kinases, including glycogen synthase kinase 3β (GSK- 3β) and at least two anchor proteins that also function as tumor suppressor proteins, namely Axin1 or Axin2 and APC (adenomatous polyposis coli). APC and Axin function as negative regulators of the pathway by sequestering β -catenin in the cytoplasm. Hence, inactivating mutations in *Apc* lead to higher β -catenin protein accumulation among other important events controlled by APC. Activation of the pathway by Wnt leads to inactivation of the destruction complex allowing buildup of β -catenin and its migration to the nucleus. In the nucleus, β -catenin binds to members of the TCF/LEF transcription factor family, thereby converting them from transcriptional repressors into transcriptional activators.

Initial attempts to overexpress a constitutively active form of β -catenin in HSCs led to an increase in proliferation and repopulation capacity upon transplantation into lethally irradiated mice (Reya et al., 2003). However, later studies using conditional overexpression of a stabilized form of β -catenin led to a block in multilineage differentiation, and the exhaustion of long-term HSCs (Kirstetter et al., 2006; Scheller et al., 2006). This resulted in anemic mice and eventually led to lethality, i.e., the opposite effect when compared with

the improved transplantation setting reported earlier. These studies have created confusion concerning the importance of Wnt in maintaining numbers and integrity of HSCs. Similarly, not all loss-of-function studies have produced clear phenotypes. The Mx-Cre system has been used to drive deletion of β -catenin (Zhao et al., 2007) or both β -catenin and its homolog γ -catenin (Koch et al., 2008; Jeannet et al., 2008). However, no defects were reported in HSC function or cells within lymphoid tissues. Surprisingly, in vivo reporter assays revealed that the canonical Wnt signaling pathway was still active in HSCs despite the absence of both β - and γ -catenin (Jeannet et al., 2008). This could imply the existence of an alternative factor or generation of a hypomorphic allele permitting low levels of Wnt signaling that would negate hematopoietic defects. Heroic efforts to knock out the *Porcn* gene during hematopoiesis, which encodes an acyltransferase (porcupine) necessary for acylation of Wnts, enabling their secretion and binding to the frizzled receptors, have not resulted in hematopoietic defects; however, there also were no changes in Wnt signaling (Kabiri et al., 2015). The reasons for this are presently unknown, but incomplete deletion or the lack of need for Wnt secretion have been suggested (Oostendorp, 2015). This demonstrates the high complexity and difficulty in generating bona fide null mutants for canonical Wnts in the hematopoietic system. Together with studies in which Wnt activity in HSCs was reported to be close to zero (Fleming et al., 2008; Luis et al., 2009; Zhao et al., 2007), these findings suggest that complete absence of Wnt signaling is detrimental to HSC function, but that up to a quarter of normal activity is sufficient for normal function. Our recent findings suggest that these very different results in both gain- of-function and loss-of-function studies can be largely explained by differences in levels of Wnt signaling achieved in different experimental circumstances. That is, when Wnt signaling is slightly enhanced over normal levels, HSCs show improved reconstitution capacity. However, when HSCs express high levels of Wnt signaling, they completely fail to reconstitute irradiated recipient mice (Luis et al., 2011). Thus, different levels of activation of the pathway can account for the discrepancies in previous studies (Malhotra and Kincade, 2009).

Results

Gene Expression Profiling and Correlation with Wnt Dosage

Previously, we have used a combination of two different hypomorphic alleles and a conditional deletion allele of the *Apc* gene resulting in a gradient of five distinct levels of Wnt signaling in vivo. In the *Apc*^{1572T} and *Apc*^{1638N} alleles, amino acid residues 1572 and 1638 have been targeted resulting in different levels and lengths of truncated *Apc* proteins, consequently leading to different levels of Wnt pathway activation. Deletion of *Apc* exon 15 within the *Apc*^{15lox} allele was performed ex vivo by using a Cre-recombinase encoding retrovirus (Figure 1A). LSK cells from wild-type (WT) mice (*Apc*^{+/+}) transduced with the same viral construct were employed as controls for all experiments. Transduced cells were sorted and employed for gene expression profiling by Affymetrix genome-wide microarrays. In the current report, we focused on the differences between WT LSK cells, which efficiently reconstitute recipient mice, and the LSK cells with increased Wnt signaling activity (*Apc*^{1572T}, *Apc*^{1638N}, and the *Apc*^{15lox} mutant alleles). Biological triplicates were used for each condition. As WT HSCs have low but detectable and slightly variable levels of Wnt signaling, and they form the basis for comparison of all other conditions, we used six replicates for WT HSCs.

Principal component analysis showed clear separation of the triplicate arrays per genotype corresponding to the different Wnt signaling levels (Figure 1B). Hierarchical clustering of the top 50 differentially expressed genes also revealed a clear separation of the different Wnt signaling clusters (Figure 1C).

Biological Processes Correlated with High Wnt Levels in HSC

Focusing on the most differentially expressed genes, a heat-map was constructed that clearly reveals the differences between WT and *Apc*^{15lox} HSCs (Figure 2A). We used the gene expression data of all available probe sets across the 15 APC samples and applied Barnes-Hut t-distributed stochastic neighbor embedding (t-SNE) to map each individual gene or probe set into a 2D space. The 2D landscape illustrates genes/probe sets with similar behavior (Figure 2B). Genes that have highly correlated expression profiles will be located in close proximity in the map, whereas uncorrelated expression profiles should be far apart in the t-SNE map. Genes that follow the increase in Wnt signaling cluster in a set of genes composed of known Wnt target genes, such as *Axin2*, *Tcf7*, and *Lef1* (Figures 2C–2F). Genes that are anti-correlated with increased Wnt signaling can also be discerned and include *Ccr9* and *Cd3g* (Figures 2G–2I).

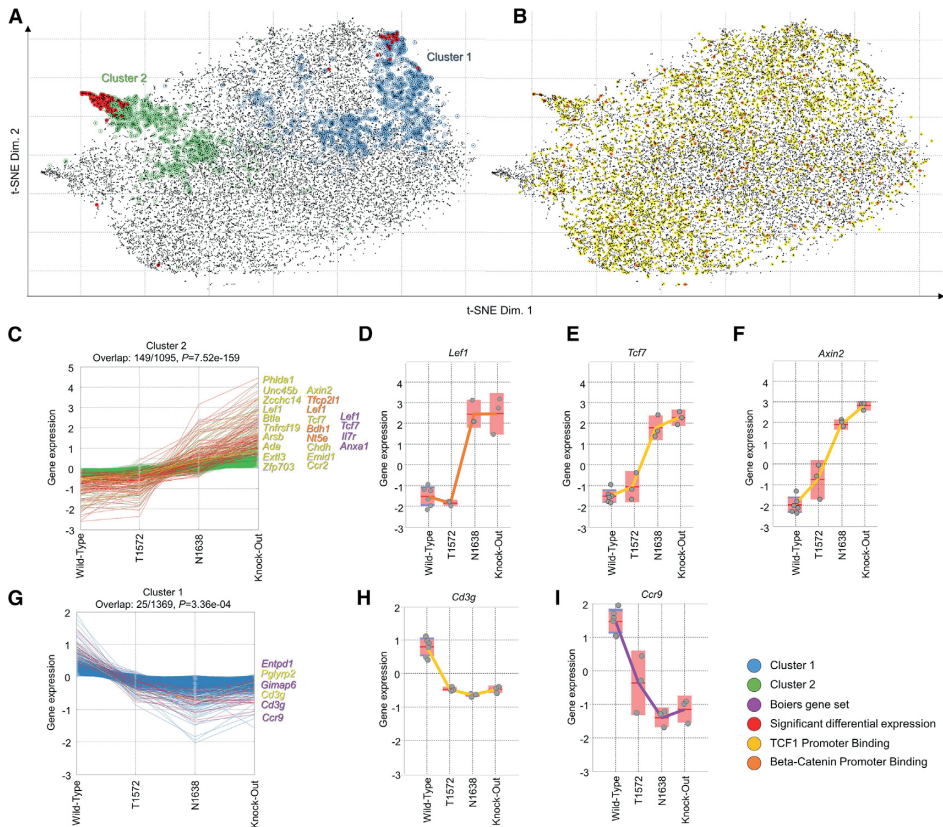


Figure 2. t-SNE Landscape of APC Mutants.

(A and B) t-SNE maps of all probe sets. Red colored lines are differentially expressed genes, green are in cluster 15, yellow show both binding (TCF1/TCF7 or β -catenin), and differential expression. Text labels are shown only for the latter. (C and G) Cluster 2 and 1 identified in t-SNE. (D–F, H, and I) Selected genes with their expression in the various *Apc* mutants.

ApC Mutants Causing High Levels of Wnt Signaling Inhibit Proliferation but Do Not Change Apoptosis

Ming et al. (2012) reported that HSCs with high Wnt signals have increased apoptosis due to a high level of Wnt signaling and impaired self-renewal in HSCs. In their study, an activated form of β -catenin was used resulting in increased Wnt signaling in HSCs to the same level as the *Apc1638N* mutant used here. We therefore also used a constitutively active β -catenin conditional allele targeted the same way as the conditional 15lox APC^{-/-} LSK cells to check the *Axin2* levels as readout for the Wnt signaling dosage. The β -catenin (Δ Ex3) allele (Harada et al., 1999) gave 21-fold higher *Axin2* levels in LSK cells compared with WT LSK cells transduced with GFP-Cre, whereas the 1638N resulted in 23-fold and the *Apc15lox* ~50-fold higher *Axin2* mRNA levels. Thus, the *Axin2* levels and hence activation of the Wnt pathway

were similar. However, our gene expression analysis did not show any significant differentially expressed genes associated with apoptosis. In order to study the putative involvement of apoptosis with a more functional approach, we performed two different apoptosis assays. First, we assessed apoptosis by annexin V/7-amino-actinomycin (7-AAD) staining of the ex vivo transduced LSK cells from *Apc* WT and *Apc*^{15lox/15lox} (Figure 3A). At the beginning of culture, there was almost no apoptosis in both groups (~4% at day 0). After 3 days of culture, the percentage of annexin V⁺ apoptotic cells increased to ~16%. However, no difference was observed between the *Apc* WT and knockout (KO) groups. Next, we performed caspase-3 staining in order to assess the apoptosis rate of ex vivo transduced LSK cells (Figure 3B). Similar to previous assays, there was hardly any caspase-3 positivity at the beginning of the culture, while it was elevated after 3 days of culture. However, again no difference was observed between the two groups. Subsequently, we analyzed the proliferation status of the transduced LSK cells by labeling the cells with proliferation dye EF670 (Figure 3C). While cells did not proliferate at the beginning of culture (filled gray histogram), *Apc* WT LSK cells proliferated around 4-fold more than *Apc* KO LSK cells. Therefore, although a high level of Wnt signaling does not affect apoptosis, it decreases proliferation of LSK cells after 3 days of culture.

High Wnt HSCs Show Enhanced Myeloid and B Lymphoid Differentiation Capacity

Our gene expression analysis revealed that LSK cells with high levels of Wnt induce upregulation of B and myeloid-associated genes (Figure S2). In order to confirm this observation functionally, we performed in vitro B and myeloid differentiation assays using the OP9 stromal cell line (Figure 4). LSK cells were sorted, transduced with the Cre-GFP retrovirus, and cultured for 14 days on OP9 cells. *Apc* lox15 LSK cells developed to granulocytes (CD11b⁺ Gr1⁺) with around 2-fold higher frequency, and developed to B cell line-age (B220⁺ CD19⁺) with around 2.5-fold higher frequency compared with WT LSK cells. Thus, we confirmed by functional assays that *Apc* mutations leading to a high level of Wnt signaling enhance differentiation toward B and myeloid lineages.

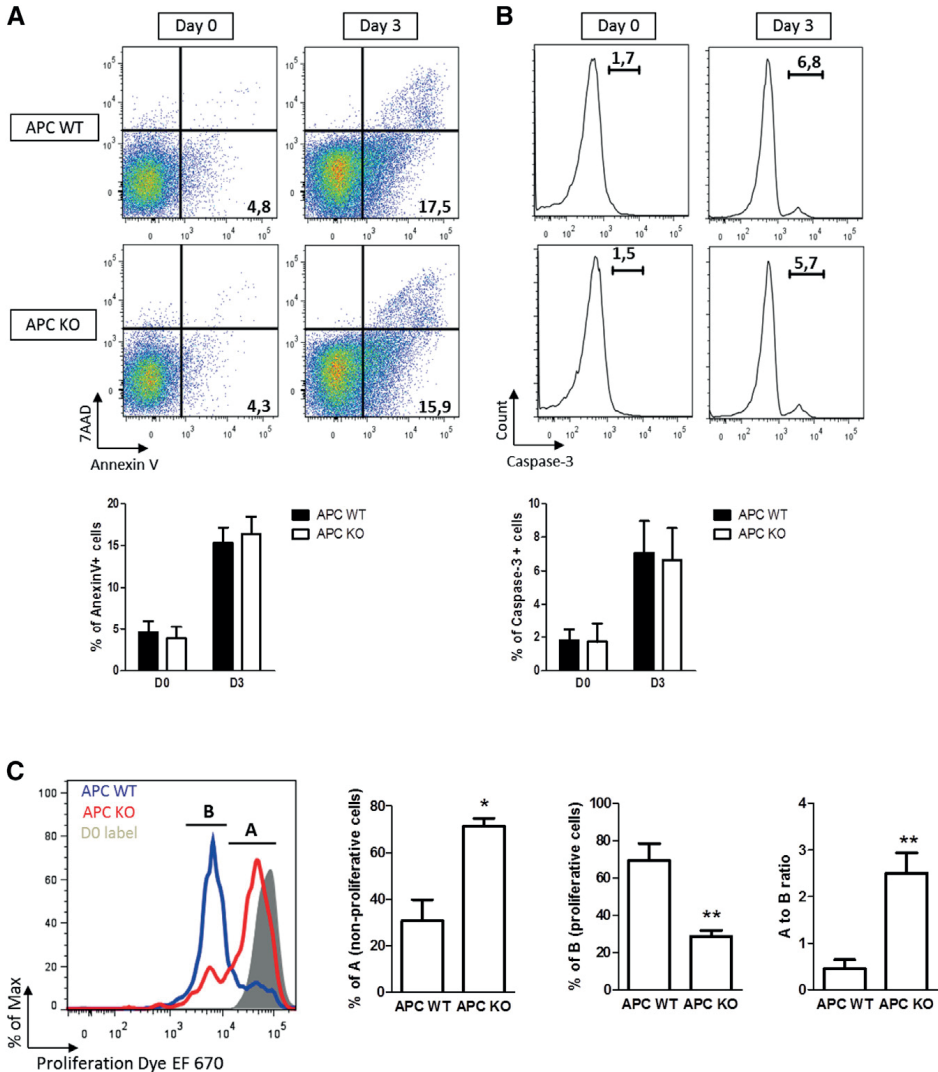


Figure 3. High Levels of Wnt Signaling Do Not Affect Apoptosis.

(A and B) Sorted BM LSK from *Apc* WT and *15lox/15lox* were transduced with Cre virus and cultured for 2 days to fulfill Cre recombination activity. After culturing for 2 days (day 0) and 5 days (day 3), cells were harvested and stained with annexin V/7-AAD (left graph) or active caspase-3 (right graph). Error bars represent the SD of three replicates of one independent experiment. (C) Sorted BM LSK from *Apc* WT and *15lox/15lox* were transduced with Cre virus, cultured for 2 days and labeled with 5 mM proliferation dye EF670 or with DMSO. The left plot depicts representative histogram plots and the right graphs show the percentage of non-proliferative cells (A), proliferative cells (B), and ratio of A/B. Error bars represent the SD of three samples from individual mice in one independent experiment. Two independent experiments were done with similar outcome. * $p < 0.05$ and ** $p < 0.01$ (Mann-Whitney U test).

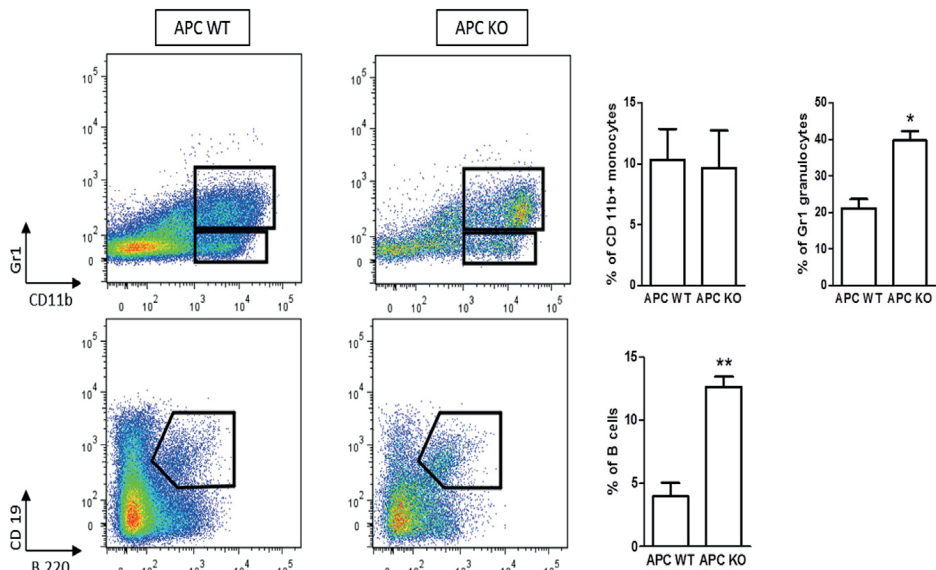


Figure 4. High Levels of Wnt Signaling Enhances Multilineage Differentiation.

Transduced LSK cells from *Apc* WT and *15lox/15lox* were co-cultured with OP9 stromal cell line for 14 days, then were harvested, and assessed by flow cytometry for myeloid (CD11b and Gr1+) and B cell development (B220 and CD19+). Error bars represent the SD of six samples from individual mice from two independent experiments. Asterisks indicate statistical significance as follows: * $p < 0.05$, and ** $p < 0.01$ (Mann-Whitney U test).

Discussion

The Wnt signaling pathway has emerged as the dominant self-renewal pathway for various adult-type stem cells and is required for maintenance of embryonic as well as induced pluripotent stem cells. In the hematopoietic system, only mild increased Wnt dosages result in higher stem cell activity; indeed the overall Wnt signaling levels in HSC are much lower than those found in intestinal, skin, or mammary gland stem cells. Nevertheless, complete loss of Wnt signaling leads to defective self-renewal as shown in secondary transplantations. This had led to interest in the use of Wnt signaling or factors that modulate Wnt signaling, such as prostaglandin E2 (PGE2) (Goessling et al., 2009) or GSK-3b inhibitors (Huang et al., 2012), for expansion of HSCs ex vivo.

We previously demonstrated that Wnt signaling functions in a strictly controlled dosage-dependent fashion (Luis et al., 2011). As also shown by several other laboratories (Kirstetter et al., 2006; Ming et al., 2012) (Scheller et al., 2006), high Wnt levels in HSCs eventually lead to stem cell exhaustion and lack of reconstitution of irradiated recipients. In the current study, we used gene expression profiling to understand why *Apc* mutations that lead to high Wnt signaling (among other defects) in HSCs would lead to loss of repopulating capacity. Our results show, both at the genetic level and in functional assays, increased differentiation, diminished proliferation, and no effects on apoptosis. The much stronger differentiation toward mature blood lineages coupled with loss of HSC proliferation (see also Figure S4) is expected to lead to lower reconstitution by HSCs. Collectively, these data explain the lack of maintaining bona fide stemness in *Apc* exon 15 deleted HSCs. Thus, instead of increased apoptosis of HSCs, here we offer another explanation for the loss of reconstitution capacity induced by high Wnt levels.

An alternative interpretation of our data is that the observed consequences of *Apc* mutant alleles are not Wnt but rather APC dependent. *Apc* encodes for a multifunctional protein involved in a broad spectrum of cellular functions (Gaspar and Fodde, 2004). To date, most *Apc* mutant mouse models are characterized by tumor phenotypes that depend completely on Wnt dosage. *Apc*1638T, the only targeted *Apc* mutation that does not affect Wnt signaling at all, results in homozygous viable and tumor-free animals, notwithstanding the deletion of the C-terminal third of the protein containing many functional domains (Smits et al., 1999, 2000). Deletion of only a few amino acids encompassing crucial Axin-binding motifs results in Wnt signaling activation, tumor formation, and lack of reconstitution by HSCs, as we have shown before (Luis et al., 2011). Finally, mutations affecting other members of the Wnt pathway, such as Gsk3 β and β -catenin, result in levels of signaling activation and hematopoietic defects that are fully in agreement with our results (Goessling et al., 2009; Huang et al., 2009, 2012; Lane et al., 2010). Therefore, the

most likely explanation is that specific levels of Wnt signaling are the major determinant of the observed differential effects on hematopoiesis. In addition, recent studies using recombinant Wnt3a also showed a dose dependent effect on HSC biology (Famili et al., 2015) where high Wnt3a leads to loss of human HSC proliferation in vitro (Duinhouwer et al., 2015), underscoring the differential effects we also have observed with the different *Apc* alleles and correlating exactly with the Wnt dosages caused by these mutations.

The finding that the *Apc* 15lox mutant leading to high Wnt signaling levels is associated with increased numbers of differentiated cells is not unprecedented. In the intestine, Wnt signaling induces maturation of Paneth cells that contain active β -catenin and Tcf4 (van Es et al., 2005), confirming that high Wnt signaling levels can drive differentiation processes.

Other investigators have used a different system to increase Wnt signals in HSCs, namely overexpression of an oncogenic, constitutively active form of β -catenin (Ming et al., 2012). They showed an increase in apoptosis using annexin V/propidium iodide staining from 10% in WT LSK cells to 35% in high Wnt LSK cells. The reasons for the differences with our results could be due to differences in the systems used, although both are expected to lead to high Wnt signaling levels. Possibly activated β -catenin also negatively affects cell adhesion and homing properties thereby decreasing exposure to important survival signals leading to increased apoptosis. It is also noteworthy that enhanced survival signals are needed to have HSCs survive in the oncogenic β -catenin system. In addition, Li et al. (2013) have shown that *Apc* regulates the function of HSCs largely through β -catenin-dependent mechanisms, thus demonstrating that, in both systems, canonical Wnt signaling is the major factor.

Whatever the exact mechanism, it is clear that Wnt signaling levels need to be strictly controlled. It is well possible that somewhat higher Wnt levels, which are detrimental to stemness, can be tolerated if HSC survival is enhanced, which then would lead to better self-renewal at this somewhat higher Wnt signaling dose. For instance PI3K/Akt signaling (Perry et al., 2011), as well as expression of Bcl2 (Reya et al., 2003) can provide such signals. Apparently, high Wnt signaling levels can be tolerated in HSC in combination with activation of other survival pathways. Intriguingly, the high Wnt levels in combination with oncogene activation in acute myeloid leukemia seem to allow the Wnt pathway to function as a self-renewal factor for leukemic stem cells (Wang et al., 2010), whereas high Wnt levels cannot do so in normal HSCs. The different localization of normal versus malignant HSCs in the bone marrow niche (Lane et al., 2011) may also contribute to this differential outcome of high Wnt dosage and opens up a therapeutic window targeting leukemic but not normal stem cells.

Experimental procedures

Mice

Mice were bred and maintained in the animal facilities of Leiden University Medical Center, in accordance with legal regulations in the Netherlands and with the approval of the Dutch animal ethical committee.

Microarray Analysis

In this study, we measured the genome-wide gene expression profiles in 21 APC C57Bl/6 mouse samples using Affymetrix mouse 430 2 microarrays for four different conditions; six APC WT, three APC 15lox/1572T, three APC 15lox/1638N, and three APC 15lox/ 15lox mice. 40,000–70,000 sorted LSK cells were stimulated over-night in serum-free medium (STEMCELL Technologies) supplemented with cytokines and transduced by spinoculation with MSCV-Cre-IRES-GFP. Subsequently, Cre-GFP-expressing LSK cells were isolated using flow cytometric cell sorting and collected for RNA expression. RNA of more than 10,000 cells was amplified and processed using the Encore Biotin module and hybridized to Affymetrix mouse 430 2.0 Genechip arrays. Differential expressed genes were determined using Limma, and genes were considered to be differentially expressed if mRNA levels differ with $p < 0.05$ after multiple test correction using Holm. The dataset associated with this study has been deposited at GEO: GSE79495.

Flow Cytometry

Cells were stained in fluorescence-activated cell sorting buffer at 4 °C, washed, and measured either on a Canto I or an Aria (BD Biosciences). Data were analyzed using FlowJo software (Tree Star).

Proliferation, Apoptosis, and Differentiation Assays

For apoptosis, cells were harvested after 2 days (day 0) or 5 days (day 3) of culture, and stained with either 7-AAD/annexin V (BD Bioscience), or phycoerythrin-active caspase-3 apoptosis kit (BD Pharmingen). For the proliferation assay, cells were labeled with 5 mM Cell Proliferation Dye eFluor 670 (eBioscience) at day 0. Subsequently, cells were harvested at day 3 and were assessed for proliferation. For differentiation assays, LSK cells were transduced at day 0 and transferred onto confluent monolayers of OP9 WT. After 14 days, cells were harvested and assessed by flow cytometry for B and myeloid lineage differentiation.

Acknowledgments

We thank Edwin de Haas for expert cell sorting and Paul Roozen for initiating this project. We thank Bjorn Clausen for help with the constitutive activated β -catenin allele. This work was supported in part by a TOP grant from The Netherlands Organization for Health Research and Development (ZonMw Project 40-00812-98-09050), a grant from the Dutch government to the Netherlands Institute for Regenerative Medicine (NIRM, grant no. FES0908), and JSH/EHA fellowship to M.H.B.

Received: October 22, 2015

Revised: April 7, 2016

Accepted: April 11, 2016

Published: May 10, 2016

Supplemental Information

Supplemental Experimental procedures

Mouse bone marrow (BM) cells were isolated from femurs and tibiae, which were crushed in a mortar and filtered through 70 μ m filters. The cells were stained using biotinylated lineage antibodies (MAC-1/CD11b, B220/CD45R, CD3e, CD4, NK1.1, Gr1, Ter119), Streptavidin PE, CD117 APC and Sca1 PECy7. LSK cells were isolated using a BD Aria II SORP cell sorter (Beckton-Dickinson) and were collected in Stemspan (Stem Cell Technologies), supplemented with mFlt3L (50 ng/ml), rmSCF (100 ng/ml) and rmTPO (10 ng/ml, all cytokines purchased from R&D systems). The cells were incubated for 16 hr at 37°C and 5% CO₂. LSKs from Apc¹⁵ Lox heterozygous mice with mildly elevated Wnt levels were shown to perform better in reconstitution experiments but are not integral part of the current study, as only subtle changes in gene expression were found.

Retroviral Production and Transduction

MSCV-Cre-IRES-GFP plasmid was kindly provided by H. Nakauchi (Institute of Medical Science, University of Tokyo, Japan) and viruses were generated with the Phoenix-packaging cell line. 40,000–70,000 sorted LSKs were stimulated overnight in serum-free medium (StemCell Technologies) supplemented with cytokines (100 ng/ml rmSCF, 10 ng/ml rmTPO, and 50 ng/ml rmFlt3L; from R&D) and transduced by spinoculation (800 x g, 2 hours, 32°C) with titrated amounts of virus with Retronectin (Takara Bio Inc.). Cells were cultured for 2 additional days. Subsequently, Cre-GFP expressing LSK cells were isolated using flow cytometry cell sorting and collected for RNA expression. For in vitro assays including apoptosis, proliferation and differentiation assays bulk of transduced and un-transduced cells were used.

RNA amplification

RNA was isolated from the sorted transduced cells using Qiagen RNEasy micro columns (Qiagen, Hilden, Germany). RNA of more than 10,000 cells were then amplified using the Ovation RNA amplification system v2 (Nugen Inc., San Carlos, CA, USA), processed using the Encore Biotin module (Nugen) and hybridized to Affymetrix mouse 430 2.0 Genechip arrays. Data is available at the NCBI Gene Expression Omnibus (GEO), accession number GSE79495.

Gene expression normalization. Gene expression data was measured in two batches. Raw data is normalized per batch with Robust Multi-Array Average (RMA), and batch correction is applied using Combat. Intensity values were mean centered per probe set. Gene symbols are mapped using MM9. As a result of the normalization, probe-intensity values follow a normal distribution for which intensities higher than 0 are up-regulated, and intensities lower than 0 are down-regulated. Principal component analysis and pairwise

correlations across the 21 samples showed the expected results; wild-type and mutants, t1572, n1638, and Knock-Out samples are different from each other in the PCA-space and correlation map.

Gene expression analysis. Differential expressed genes for the APC samples are determined by using Limma, and genes are considered to be differential expressed between the two selected groups if mRNA levels differ with $P < 0.05$ after multiple test correction using Holm.

ChIP-Seq normalization. In this study we used massively parallel sequenced DNA-fragments bound by the transcription factors, TCF1, TCF7, and β -catenin. All the sequencing data is aligned using Burrows-Wheeler transformation (BWA), according MM9. We used several literature sources (Li et al., 2013a; Steinke et al., 2014; Zhang and Li, 2008; Zhang et al., 2000) (Wu et al., 2012).

ChIP-Seq analysis. Binding of transcription factors is determined by utilizing Hypergeometric Analysis of Tilling arrays (HATSEQ). A binding event was called when fragments are enriched based on default parameter settings, i.e., FWER significance level < 0.05 , and a bandwidth (fragment size) of 300bp. We mapped the significantly detected binding sites to RefSeq genes in UCSC mm9 database (genome.ucsc.edu). A gene was designated as the target gene if the peak was present within 5000bp upstream of the transcription start site or inside of the gene.

For TCF1 (in mature CD8 T cells, accession number GSM1258235), we detected 591 significantly enriched regions (ranges between 104bp-1048bp, median: 233bp) by comparing it to control IgG using sorted post-select DP and CD4+8lo thymocytes1 (accession number GSM1258236). The detected regions could subsequently be mapped to 116 unique genes. For the two TCF1 experiments in murine thymocytes (GSM1285796 for TCF1-CAT and GSM1133644 for TCF1), we detected 732 (size ranges between 102bp- 2632bp, median: 237bp), and 2600 (102bp-2632bp, median: 237bp) significant binding regions respectively after comparing to control TCF1-CAT-INPUT (GSM1285797) and TCF1-INPUT (GSM1133645) respectively. The detected regions could subsequently be mapped to respectively 131, and 653 unique genes (Table S2). The third analyzed ChIP-Seq data set was the binding of TCF7 (GSM773994). For TCF7 we detected 6395 significant binding regions (size ranges between 103bp-5840bp, median: 341bp) by comparing it to one control (input DNA of TCF7). These regions are subsequently mapped to 2015 genes (Table S2). The fourth public data set that we analyzed were three Beta-Catenin experiments, two with biotinylation and one based on FLAG-tag technology. As a background four different controls are used per experiment (2 with Beta-Catenin biotin without GSK and two GSK input samples). This resulted in

respectively 990, 385, and 671 significant binding regions for Beta-Catenin-Biotin-rep1, Beta-Catenin-Biotin-rep2, and Beta-Catenin- Flag-rep1 and were mapped to 121, 49, and 79 genes (Table S2). Binding sites have median size of 336bp, 385bp, and 320bp.

To test the validity of the detected binding regions of each experiment, we expected an overrepresentation of WNT-associated genes. To test this, we overlaid the mapped genes with known WNT-associated genes (n=1136) from the Molecular Signature Database (MSigDB, v4.0), and detected that all seven ChIP-seq experiment showed a significant enrichment for binding in close vicinity of WNT-associated genes ($P < 0.05$, Table S1) based on the hypergeometric test. As an example, all seven experiments showed binding of in the transcriptional start site of *Axin2* (Figure S4A), whereas TCF1, and Beta-Catenin experiments showed also binding for *Lef1* (Figure S4A).

Pathway Analysis. Pathway analysis is performed by utilizing the Molecular Signature Database (MSigDB, v4.0) for the detection of enriched curated gene sets (C2), motif gene sets (C3), computational gene sets (C4), GO gene sets (C5), oncogenic signatures (C6), and immunologic signatures (C7). Gene sets and signatures are considered statistically significant when the P-value, derived from the hypergeometric test, is less or equal than 0.05 after correcting for multiple testing using Holm.

Mice

Mice were bred and maintained in the animal facilities of Leiden University Medical Center, in accordance with legal regulations in The Netherlands and with the approval of the Dutch animal ethical committee. C57Bl/6-CD45.1 (Ly5.1) and C57Bl/6-CD45.2 (Ly5.2) mice were obtained from the Jackson Laboratory. Mice carrying targeted mutations on *Apc* were previously described (Fodde et al., 1994; Robanus-Maandag et al., 2010; Smits et al., 1999) and continuously backcrossed to C57Bl/6 background.

Flow Cytometry

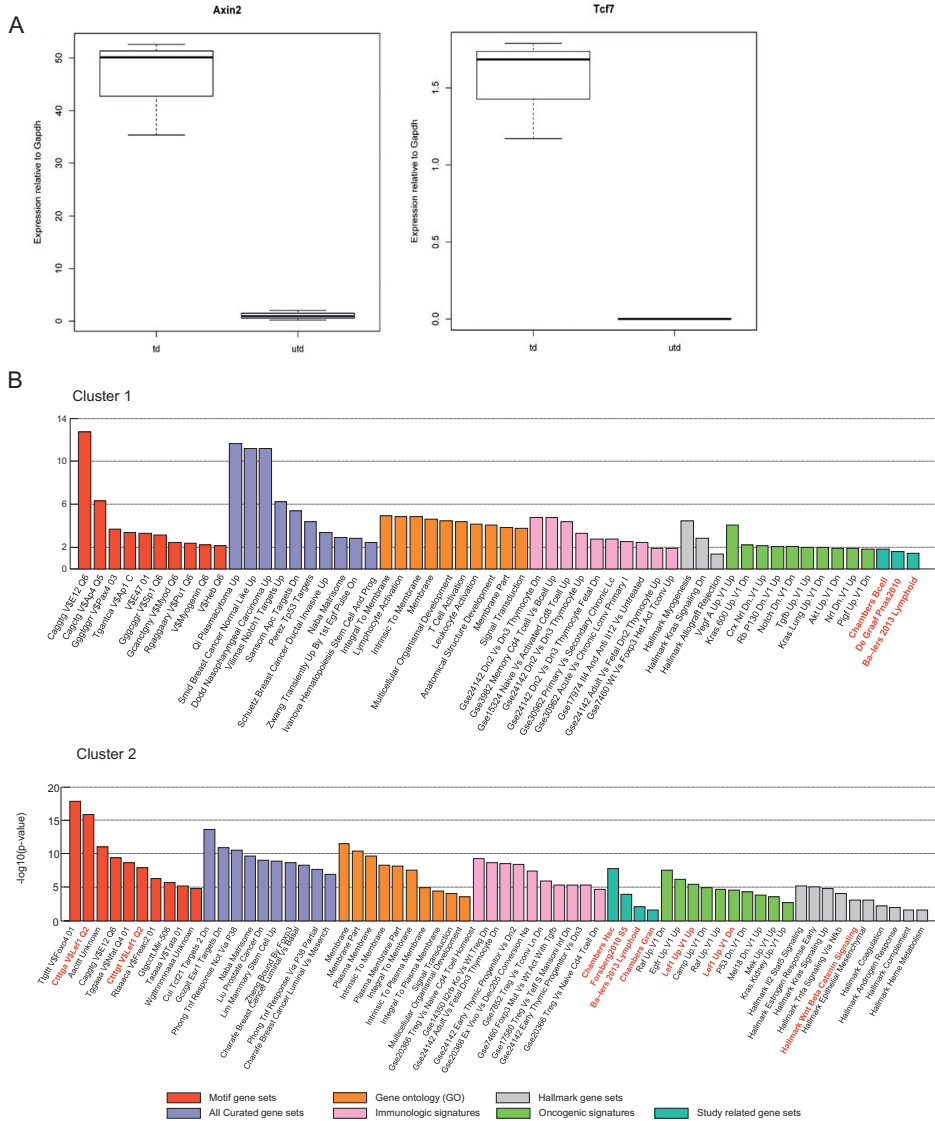
The following antibodies were obtained from BD Biosciences (San Diego, CA): anti CD11b-PE (M1/70), anti CD19-APC (ID3) and anti CD117 (2B6). For Lineage depletion these markers were used: CD3 (145-2C11), CD4 (L3T4), CD8 (53-6.7), CD11b (M1/70), Gr1 (RB6-8C5), B220 (Ra3-6B2), Ter119 (Ly76) and Nk1.1 (PK136) biotin and subsequently were stained with streptavidin eFluor 450 (48-4317) from eBioscience. The following antibodies were also purchased from eBiosciences: B220 PE-Cy7 (RA3-6B2), Gr1 eFluor 450 (RB6-8C5) and Sca1 PE-Cy7 (D7). Cells were stained in Fluorescence activated cell sorter (FACS) buffer (PBS, 2% bovine serum albumin, 0.1% sodium azide) for 30 min at 4 °C. Ultimately, Cells were washed and measured either on a Canto I, or an Aria (BD Biosciences). Data were analyzed using FlowJo software (Tree Star, Ashland, OR, USA).

Proliferation, apoptosis and differentiation assays

5 × 10⁴ sorted BM LSKs from APC WT and APC 15lox/15lox mice were transduced with titrated amount of CRE viruses in stemspan with FTS cytokines as previously described. For apoptosis assay harvested cells after 2 days (Day 0) or 5 days (Day 3) of culture, cells were stained with either 7AAD/AnnexinV (BD Bioscience), or PE-Active caspase-3 apoptosis kit (BD pharmingen) according to the manufacturer's instruction. For proliferation assay, cells were labelled with 5 uM Cell Proliferation Dye eFluor® 670 (eBioscience) at Day 0. Subsequently, cells were harvested at Day 3 and were assessed by flow cytometry for proliferation.

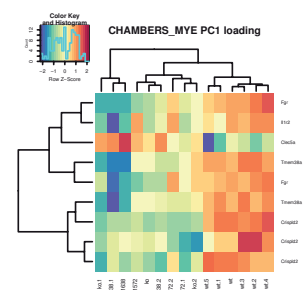
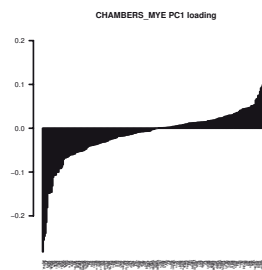
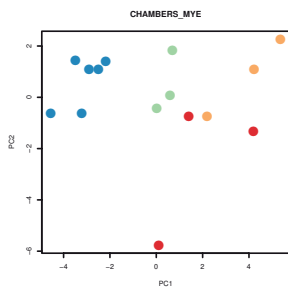
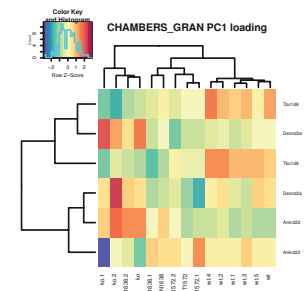
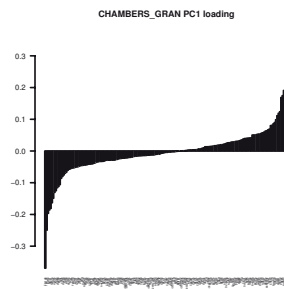
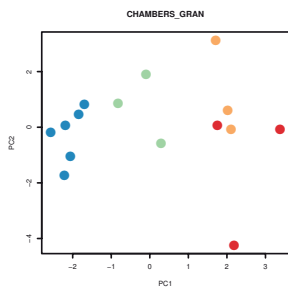
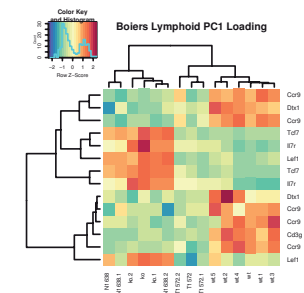
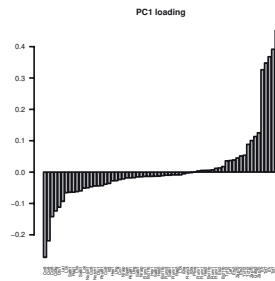
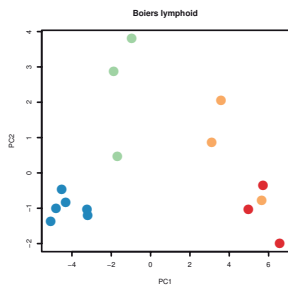
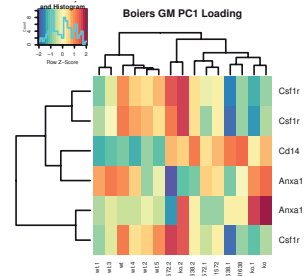
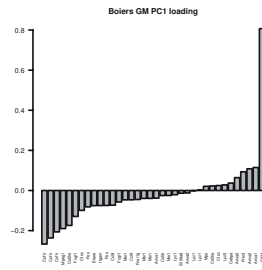
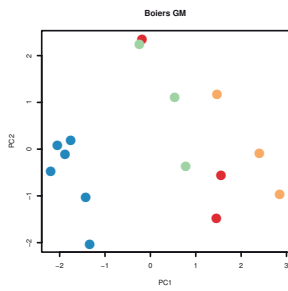
For differentiation assay 2 × 10⁴ BM LSKs were used and transduced cells at Day 0 were transferred onto confluent monolayers of OP9 WT and cocultured for additional 14 days with AlphaMEM 10% FCS containing 50 ng/ml rmSCF, 10 ng/ml rmFlt3L and 10 ng/ml rmIL-7 (all cytokines from R&D). After 7 days cells were harvested and transferred onto new monolayer of OP9 cells, and half of the medium were replaced every 3-4 days. Finally, after 14 days of coculture cells were harvested and assessed by flow cytometry for B and myeloid lineage differentiation.

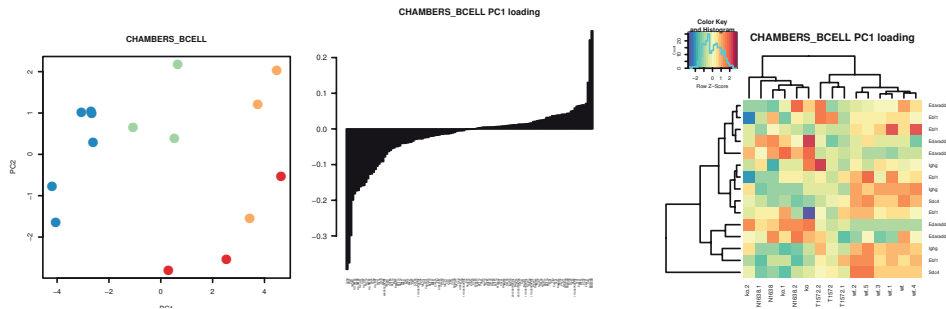
Supplemental Figures



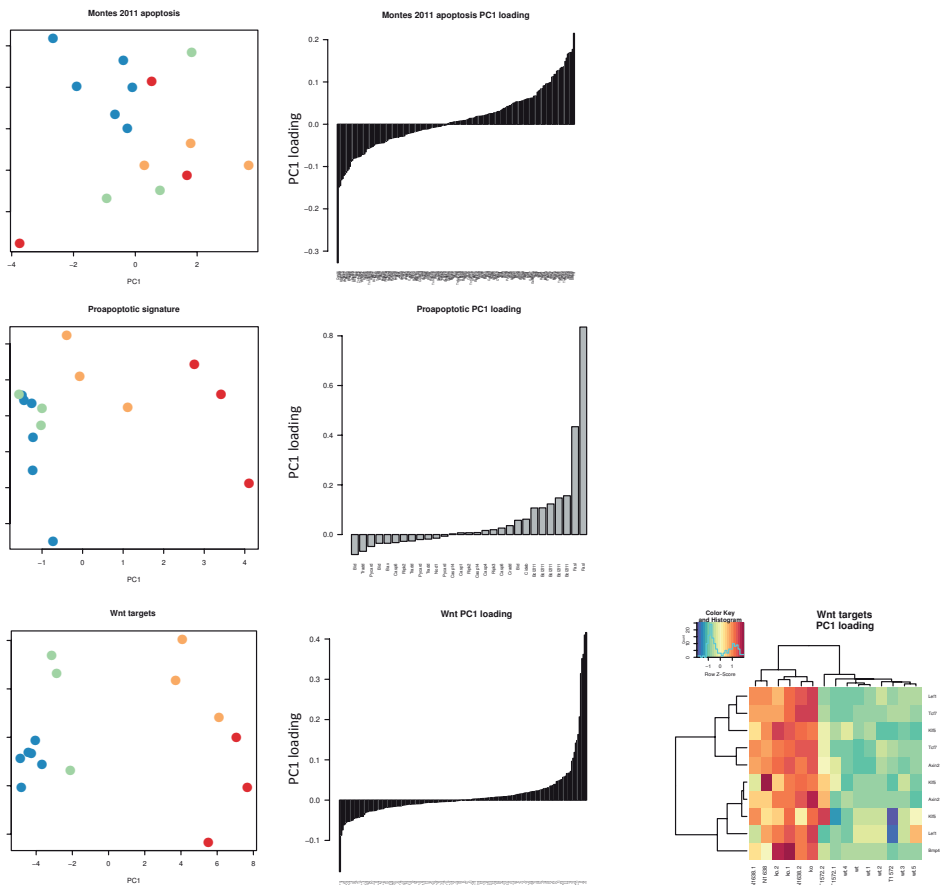
Suppl. Fig 1a: Validation of differential gene expression by Q-PCR. Sorted LSK cells were cultured and transduced with CRE-GFP as described in the supplemental experimental procedures. RNA was isolated and used for analysis by Q-PCR for the indicated Wnt target genes.

Suppl. Fig 1b: Biological processes associated with clusters 1 and 2. For details see text





Suppl. Fig 2: High Wnt signaling is associated with differentiation into monocytes and B lymphocytes based on published gene sets.



Suppl. Fig 3: No differences in apoptosis and cell cycle in high Wnt signature when compared to published gene sets.

Table S1

Gene-set	Pathway	P _{adj} < 0.05	Genes
All Curated gene sets	MATSUDA, NATURAL_KILLER_DIFFERENTIATION	6.68E-06	ANKA1, APCDD1, CCR9, CD160, CDC23, GPR34, IL2RB, MYO5A, NTRK3, PDCD1, PLAGL1, PRSS23, PTFR, PVR, SH3BGR2, SYTL2, TCF7, TULP3, XCL1, ZCCHC12C
All Curated gene sets	PICCALUGA, ANGIOIMMUNOBLASTIC_LYMPHOMA_UP	0.0002209	ANTXR1, CD93, CLU, DCLK1, FN1, FSTL1, IL18, LAMC1, PLA2G4C, RA14, THEM163, TNS1, BEND5, CHST2, CLU, CRISPLD2, EPAS1, GPR155, ITGA2, PHLD4, PLAGL1, PRSS23, RHOG, ROBO1, TF, CP2L1, THEM35, TNS1, WIJ, ZCCHC14
All Curated gene sets	LIU, PROSTATE_CANCER_DN	0.0002209	ALDH1A3, ANKX1, CHST2, DPP4, ENTDP1, FN1, IGSF3, ITGA2, MED13, NR2P, NTSE, PH4A2, PRSS23, PT, PRF, S100A5, STX3
All Curated gene sets	DELVS, THYROID_CANCER_UP	0.0006965	APC, AXIN2, DKF2, FSTL1, NKD1, WIF1
All Curated gene sets	ST, WNT, BETA, CATENIN_PATHWAY	0.001009	ANTXR1, ANKX1, CLU, EPAS1, GIMAP6, NTSE, PHLD4, RHOG
All Curated gene sets	SANA, TNF_SIGNALING_DN	0.001009	ABHD2, CLU, DCLK1, FETUB, GRAF1, GPC4, MB21D2, MYO5A, PPAP2A, PRSS23, RASGRP1, RN144B, SDK1, SH3BGR2, SHROOM3, SIPA1L2, SYTL2, THBD, THSD4
All Curated gene sets	GOZGIT, ESR1_TARGETS_DN	0.001305	ANTXR1, APCDD1, ARS5, BMP4, BMPER, CLU, DCLK1, EMD1, FN1, GAS2L3, HUNK, KLF5, LYPO6B, NKD1, NR2P
All Curated gene sets	CU1, TCF21_TARGETS_2_UP	0.001305	ENTDP1, IL18, LAMC1, NTSE, SYTL2
All Curated gene sets	GAVIN, PDE3B_TARGETS	0.001305	ADAM22, ANKX1, BMP1, BMPER, CRISPLD2, ELFN1, EMD1, FN1, FREM2, FST, FSTL1, GPC4, IL18, ISM1, KY, LAMC1, PH4A2, S100A5, SCUBE3, THSD4, WIF1, XCL1
All Curated gene sets	NABA, MATRISOME	0.003449	APC, AXIN2, CAMK2D, DKF2, LEF1, NFATC2, NKD1, TCF7, WIF1
All Curated gene sets	KEGG_WNT_SIGNALING_PATHWAY	0.00359	CANXD2, CDCD109B, FST, IL18, LYPO6B, PACSIN1, PRSS23, TNFRSF19
All Curated gene sets	CERIVERA, SDHS_TARGETS_1_UP	0.005222	CAMK2D, DCLK1, DCLK1, FAM83A, FN1, FSTL1, LAMC1, MB21D2, NTSE, PHLD4, PRSS23, SIPA1L2
All Curated gene sets	KINSEY_TARGETS_OF_EWSR1_FLII_FUSION_DN	0.005222	ADLA, ALDH1A3, ANTXR1, ANKX1, CD14, FST, FSTL1, IL18, IL7R, IGSF3, LAMC1, NTSE, PHLD4, ZCCH12C
All Curated gene sets	CHARAFE, BREAST_CANCER_LIMINAL_VS_BASAL_DN	0.005292	ABHD2, ALDH1A3, BACE1, BMP4, CLU, FST, NR2P, PHLD4, TNFRSF19
All Curated gene sets	RIGGI, EWING_SARCOMA_PROGENITOR_DN	0.007768	AXIN2, LEF1, NKD1, TCF7, TNFRSF19, WIF1
All Curated gene sets	SANSOM, WNT_PATHWAY_REQUIRE_MYC	0.008652	ADLA, ANTXR1, ENTDP1, IRF4, NUDT1, OSBP1A, PHLD4, PVR, SH3BGR2, SHROOM3, TULP3
All Curated gene sets	PASQUALUCCI, LYMPHOMA_BY_GC_STAGE_UP	0.008714	AXIN2, CD4, CHST2, EPAS1, GPR34, FST, FAM83A, GRAF1, GPC4, IL2RB, KIF5C, LEF1, MYO5A, PDCD1, STX3, SULT14, TFCP2L1, TFCP2L1, TULP3, XCL1
All Curated gene sets	BYSTRYKH, HEMATOPOIESIS_STEM_CELL_QTL_TRANS	0.008714	ARHGAP28, ARS5, BMP4, BMPER, FST, GPC4, IL18, NTSE, TEK
All Curated gene sets	GAUSSMANN, MLL_A4_FUSION_TARGETS_F_UP	0.009692	CDCD109B, CD83, EPAS1, IL2RB, LYPO6B, PLAGL1, SH3BGR2
All Curated gene sets	GAVIN, FOXP3_TARGETS_CLUSTER_P4	0.01055	CCR2, CR2, CD93, CLU, DCLK1, FN1, IL2RB, IL7R, TNFRSF19, TNFRSF25, XCL1
All Curated gene sets	KEGG_CYTOKINE_CYTOKINE_RECEPTOR_INTERACTION	0.01299	ABHD2, ALDH1A3, ANKX1, APCDD1, ATP13A4, BACE1, BDN1, BEND5, CANXD2, CLU, EDAR, EPAS1, FAM63A, FMN1, IL18, KLF5, LYPO6B, PKRKA2, PRSS23, SH3BGR2, SMDP3, SNK31, SYTL2, TNFRSF19, TNS1, TUBB3
All Curated gene sets	DODD, NASOPHARYNGEAL_CARCINOMA_UP	0.01525	BMPER, CDCD101, CRISPLD2, DCLK1, EFHD1, FREM2, GRAF1, ITGA2, MB21D2, MYO5A, PRSS23, SYTL2, THSD4, TPDS2L1
All Curated gene sets	CREIGHTON, ENDOCRINE_THERAPY_RESISTANCE_1	0.01646	CCR2, CDCD109B, CLU, DPP4, GIMAP6, IL7R, LEF1, NTSE, SNCAIP, THBD, TNFRSF25, WIF1, XCL1
All Curated gene sets	SMID, BREAST_CANCER_NORMAL_LIKE_UP	0.01783	SH4D1, IL7R, IL2RB, CLU, EPAS1, BACE1, CDCD109B, THBD, TNS1
All Curated gene sets	SMID, BREAST_CANCER_NORMAL_LIKE_UP	0.01851	CDCD109B, CD83, CD93, CLU, DCLK1, GIMAP6, IL7R, RASGRP1, THBD, THEM35
All Curated gene sets	WALLACE, PROSTATE_CANCER_RACE_UP	0.01852	CARD11, CCR2, CD3G, CLU, DPP4, IL7R, IL18, IL2RB, TUBB3, XCL1
All Curated gene sets	UP, PLASMACYTOMA_UP	0.02286	ABHD2, DCLK1, FST, ITGA2, NUDT1, PTFR, PVR, TUBB3
All Curated gene sets	AMIT, EGF_RESPONSE_480_HELA	0.02337	ADAM22, ANKX1, BMP4, ELFN1, FREM2, FST, FSTL1, GPC4, IL18, ISM1, KY, PH4A2, S100A5, SCUBE3, WIF1, XCL1
All Curated gene sets	NABA, MATRISOME_ASSOCIATED	0.03018	BTAK, CAMK2D, CARD11, CCR2, CD14, CD160, CD3G, CDC23, IL18, IL2RB, IL7R, IRF4, OSBP1A, PDCD1, PVR, RASGRP1, RASGRP1, RN144B
All Curated gene sets	REACTOME_IMMUNE_SYSTEM	0.03141	ABHD2, CD83, CHST2, FN1, IL7R, IRF4, MB21D2, MYO5A, NR3P3, PH4A2, PHLD4, RA14, RASGRP1, THBD
All Curated gene sets	FULCHER, INFLAMMATORY_RESPONSE_LECTIN_VS_LPS_UP	0.03141	ALDH1A3, ANKX1, BDN1, CLU, CRISPLD2, EDARADD, GPR155, NTSE, PFBP26, SULT1A1, TFCP2L1, TPDS2L1, WIF1
All Curated gene sets	SCHAEFFER, PROSTATE_DEVELOPMENT_48HR_UP	0.03313	ACTN2, APC, BACE1, CACNA1B, CACNA1D, CARD11, CCR2, CCR9, CD14, CD160, CD83, CDK5R1, DCLK1, ENTDP1, GPC4, GPR34, IL17RB, ITGA2, NTRK3, PRG1, PVR, RN144B, ROBO1, SHROOM3, STX3, SYTL2, TEK, THBD, TNFRSF25
All Curated gene sets	KIM, MYC_AMPLIFICATION_TARGETS_DN	0.03336	ACTN2, APC, BACE1, CACNA1B, CACNA1D, CARD11, CCR2, CCR9, CD14, CD160, CD83, CDK5R1, DCLK1, ENTDP1, GPC4, GPR34, IL17RB, ITGA2, NTRK3, PRG1, PVR, RN144B, ROBO1, SHROOM3, STX3, SYTL2, TEK, THBD, TNFRSF25
All Curated gene sets	LM, MAMMARY_STEM_CELL_UP	0.04392	ACTN2, APC, BACE1, CACNA1B, CACNA1D, CARD11, CCR2, CCR9, CD14, CD160, CD83, CDK5R1, DCLK1, ENTDP1, GPC4, GPR34, IL17RB, ITGA2, NTRK3, PRG1, PVR, RN144B, ROBO1, SHROOM3, STX3, SYTL2, TEK, THBD, TNFRSF25
All Curated gene sets	KEGG_BASAL_CELL_CARCINOMA	0.04682	ACTN2, APC, BACE1, CACNA1B, CACNA1D, CARD11, CCR2, CCR9, CD14, CD160, CD83, CDK5R1, DCLK1, ENTDP1, GPC4, GPR34, IL17RB, ITGA2, NTRK3, PRG1, PVR, RN144B, ROBO1, SHROOM3, STX3, SYTL2, TEK, THBD, TNFRSF25
All Curated gene sets	TAKEDA, TARGETS_OF_NUP98_HOXA9_FUSION_8D_DN	0.0468	ACTN2, APC, BACE1, CACNA1B, CACNA1D, CARD11, CCR2, CCR9, CD14, CD160, CD83, CDK5R1, DCLK1, ENTDP1, GPC4, GPR34, IL17RB, ITGA2, NTRK3, PRG1, PVR, RN144B, ROBO1, SHROOM3, STX3, SYTL2, TEK, THBD, TNFRSF25
All Curated gene sets	LINDGREN, BLADDER_CANCER_CLUSTER_2B	0.0468	ACTN2, APC, BACE1, CACNA1B, CACNA1D, CARD11, CCR2, CCR9, CD14, CD160, CD83, CDK5R1, DCLK1, ENTDP1, GPC4, GPR34, IL17RB, ITGA2, NTRK3, PRG1, PVR, RN144B, ROBO1, SHROOM3, STX3, SYTL2, TEK, THBD, TNFRSF25
All Curated gene sets	NUYTEN, EZH2_TARGETS_UP	0.0468	ACTN2, APC, BACE1, CACNA1B, CACNA1D, CARD11, CCR2, CCR9, CD14, CD160, CD83, CDK5R1, DCLK1, ENTDP1, GPC4, GPR34, IL17RB, ITGA2, NTRK3, PRG1, PVR, RN144B, ROBO1, SHROOM3, STX3, SYTL2, TEK, THBD, TNFRSF25
All Curated gene sets	SCHAEFFER, PROSTATE_DEVELOPMENT_48HR_DN	0.0468	ACTN2, APC, BACE1, CACNA1B, CACNA1D, CARD11, CCR2, CCR9, CD14, CD160, CD83, CDK5R1, DCLK1, ENTDP1, GPC4, GPR34, IL17RB, ITGA2, NTRK3, PRG1, PVR, RN144B, ROBO1, SHROOM3, STX3, SYTL2, TEK, THBD, TNFRSF25
Computational gene sets	MODULE_46	2.83E-06	ADA, CCR2, CCR9, CD14, CD3G, CD83, CDK5R1, CLU, DPP4, ENTDP1, FN1, IL18, IL2RB, IL7R, PH4A2, PDC1, XCL1
Computational gene sets	MODULE_75	2.83E-06	ADA, CCR2, CCR9, CD14, CD3G, CD83, CDK5R1, CLU, DPP4, FN1, IL18, IL2RB, IL7R, PH4A2, PDCD1, TEK, XCL1
Gene ontology (GO)	PLASMA_MEMBRANE_PART	0.000438	ACTN2, APC, BACE1, CACNA1B, CACNA1D, CARD11, CCR2, CCR9, CD14, CD160, CD83, DCLK1, ENTDP1, GPC4, GPR34, IL17RB, ITGA2, NTRK3, PRG1, PVR, RN144B, ROBO1, SHROOM3, STX3, SYTL2, TEK, THBD, TNFRSF25
Gene ontology (GO)	MEMBRANE	0.0006684	ACTN2, APC, BACE1, CACNA1B, CACNA1D, CARD11, CCR2, CCR9, CD14, CD160, CD83, CDK5R1, DCLK1, ENTDP1, GPC4, GPR34, IL17RB, ITGA2, NTRK3, PRG1, PVR, RN144B, ROBO1, SHROOM3, STX3, SYTL2, TEK, THBD, TNFRSF25
Gene ontology (GO)	PLASMA_MEMBRANE	0.0007698	ACTN2, APC, BACE1, CACNA1B, CACNA1D, CARD11, CCR2, CCR9, CD14, CD160, CD83, CDK5R1, DCLK1, ENTDP1, GPC4, GPR34, IL17RB, ITGA2, NTRK3, PRG1, PVR, RN144B, ROBO1, SHROOM3, STX3, SYTL2, TEK, THBD, TNFRSF25
Gene ontology (GO)	MEMBRANE_PART	0.001722	ACTN2, APC, BACE1, CACNA1B, CACNA1D, CARD11, CCR2, CCR9, CD14, CD160, CD83, CDK5R1, DCLK1, ENTDP1, GPC4, GPR34, IL17RB, ITGA2, NTRK3, PRG1, PVR, RN144B, ROBO1, SHROOM3, STX3, SYTL2, TEK, THBD, TNFRSF25
Gene ontology (GO)	SIGNAL_TRANSDUCTION	0.007247	ASHG, ANKX1, CCR2, CCR9, CD14, CD160, CD83, CDK5R1, DCLK1, ENTDP1, GPC4, GPR34, IL17RB, ITGA2, NTRK3, PRG1, PVR, RN144B, ROBO1, SHROOM3, STX3, SYTL2, TEK, THBD, TNFRSF25
Gene ontology (GO)	RESPONSE_TO_EXTERNAL_STIMULUS	0.01613	ASHG, ANKX1, CCR2, CCR9, CD14, CD160, CD83, CDK5R1, DCLK1, ENTDP1, GPC4, GPR34, IL17RB, ITGA2, NTRK3, PRG1, PVR, RN144B, ROBO1, SHROOM3, STX3, SYTL2, TEK, THBD, TNFRSF25
Gene ontology (GO)	RECEPTOR_ACTIVITY	0.01613	ASHG, ANKX1, CCR2, CCR9, CD14, CD160, CD83, CDK5R1, DCLK1, ENTDP1, GPC4, GPR34, IL17RB, ITGA2, NTRK3, PRG1, PVR, RN144B, ROBO1, SHROOM3, STX3, SYTL2, TEK, THBD, TNFRSF25
Hallmark gene sets	HALLMARK_ESTROGEN_RESPONSE_EARLY	0.004103	ABHD2, CLU, DCLK1, FETUB, GRAF1, GPC4, MB21D2, MYO5A, PPAP2A, PRSS23, RASGRP1, RN144B, THSD4, TPDS2L1
Hallmark gene sets	HALLMARK_INFLAMMATORY_RESPONSE	0.006397	CD14, CHST2, IL18, IL2RB, IL7R, PVR, RASGRP1, RN144B
Hallmark gene sets	HALLMARK_COAGULATION	0.006397	ANKX1, CLU, DPP4, FN1, ITGA2, PRSS23, THBD
Hallmark gene sets	HALLMARK_IL2_STATS_SIGNALING	0.006397	CD83, IL2RB, IRF4, NTSE, PHLD4, PLAGL1, PPAP2A, SH3BGR2
Hallmark gene sets	HALLMARK_WNT_BETA_CATENIN_SIGNALING	0.01107	AXIN2, LEF1, NKD1, TCF7
Hallmark gene sets	HALLMARK_COMPLEMENT	0.01636	ACTN2, CDK5R1, CLU, DPP4, FN1, CNKIP2, RASGRP1
Immunologic signatures	GSE20386_EX_VIVO_VS_DEC205_CONVERSION_NAIVE_CD4_TCELL_UP	0.001054	ACTN2, CCR2, CD160, EPAS1, GPR14, GPR34, IL17RB, RASGRP1, THBD, XCL1, XKRX
Immunologic signatures	GSE24142_EARLY_THYMIC_PROGENITOR_VS_DN2_THYMOCYTE_DN	0.001054	ADA, AXIN2, CDCD109B, CD3G, DPP4, EDARADD, IL17RB, IL7R, PDCD1, PTFR, PVR, TUBB3
Immunologic signatures	GSE7852_TREG_VS_TCONV_LN_UP	0.001054	CCR2, CD83, ENTDP1, FGD6, IRF4, LAMC1, NTSE, PLAGL1, PPAP2A, ZCCH12C, ZDHHC23
Immunologic signatures	GSE10325_LUPUS_CD4_TCELL_VS_LUPUS_BCELL_UP	0.003344	ANKX1, CDCD109B, CD3G, DPP4, GIMAP6, IL7R, LEF1, TCF7, TNFRSF25, ZCCHC14
Immunologic signatures	GSE1092_PRIMARY_VS_SECONDARY_CHRONIC_LCMV_INF_CD8_TCELL_UP	0.003344	ASHG, ANKX1, CCR2, ENTDP1, EPAS1, GPR14, GPR34, PRKAA2, RASGRP1, THEM163
Immunologic signatures	GSE24142_EARLY_THYMIC_PROGENITOR_VS_DN2_THYMOCYTE_ADULT	0.004089	AXIN2, CDCD109B, CD3G, EDARADD, IL17RB, IL7R, LEF1, PPAP2A, PTFR, PVR, SYTL2
Immunologic signatures	GSE7460_TCONV_VS_TREG_LN_DN	0.004089	CD83, DPP4, ENTDP1, IL2RB, IRF4, NTSE, PPAP2A, SH3BGR2, ZCCH12C, ZDHHC23
Immunologic signatures	GSE20386_EX_VIVO_VS_DEC205_CONVERSION_NAIVE_CD4_TCELL_DN	0.0137	ANKX1, CDCD109B, CD83, DCLK1, IL18, PLAGL1, RN144B, SNK31, STX3
Immunologic signatures	GSE10325_CD4_TCELL_VS_BCELL_UP	0.01559	ANKX1, CCR2, CD3G, DPP4, GIMAP6, IL7R, LEF1, RASGRP1, TNFRSF25
Immunologic signatures	GSE24142_EARLY_THYMIC_PROGENITOR_VS_DN3_THYMOCYTE_DN	0.01559	ADA, CDCD109B, GRAF1, IL7R, LEF1, PDCD1, PTFR, TUBB3, TULP3
Immunologic signatures	GSE39820_CTRL_VS_IL18_IL6_IL23A_CD4_TCELL_UP	0.01559	CDCD109B, CD83, IGSF3, IL2RB, KIF5C, NR2P, PLAGL1, PPAP2A, SH3BGR2
Immunologic signatures	GSE7460_TCONV_VS_TREG_THYMUUS_DN	0.01634	CCR2, CCR9, CD83, IGSF3, KIF5C, PDCD1, PLAGL1, PPAP2A, SH3BGR2
Immunologic signatures	GSE7852_TREG_VS_TCONV_THYMUUS_UP	0.01649	CCR9, CD3G, GRAF1, IRF4, LEF1, PHLD4, PTFR, TBC1D8, TULP3
Immunologic signatures	GSE24142_DN2_VS_DN3_THYMOCYTE_DN	0.03801	CDL1, DPP4, IL7R, ITGA2, PH4A1, PRKAA2, TCF7, TNS1
Immunologic signatures	GSE3982_MEMORY_CD4_TCELL_MEMORY_CD4_TCELL_DN	0.04586	ANKX1, CCR2, CD3G, DPP4, GIMAP6, IL2RB, KIF5C, PHLD4
Immunologic signatures	GSE3982_MEMORY_CD4_TCELL_VS_BCELL_UP	0.04586	ANKX1, APC, AXIN2, BDN1, BMP4, CDCD109B, CD83, DCLK1, EDAR, ENTDP1, EXTL3, FAM83A, FN1, FST, FSTL1, GRAF1, IL18, IL7R, IRF4, ITGA2, CNKIP2, KLF5, LAMC1, NKD1, NR2P, NTRK3, RN214, ROBO1, SCU3, SED1, SMDP3, SNCAIP, SYTL2, TEK, TNFRSF19, XKRX, ZCCH14
Motif gene sets	TTGTTT_VF0XO4_01	0.0001493	ABHD2, CLU, DCLK1, FETUB, GRAF1, GPC4, MB21D2, MYO5A, PPAP2A, PRSS23, RASGRP1, RN144B, THSD4, TPDS2L1
Motif gene sets	CTTTGA_V5LEF1_Q2	0.0001493	ANTXR1, BAGALTS, BMP4, CHDH, DCLK1, DNK2, DCLK1, EFHD1, FN1, FST, FSTL1, GALNT7, IGSF3, IL17RB, IL7R, IRF4, ITGA2, CNKIP2, KLF5, MED13, NFATC2, SCUBE3, SH3BGR2, SMDP3, SNCAIP, TBC1D8, TM, EM163, THEM35, TNFRSF19, TNS1, XKRX
Motif gene sets	VSTGFAA_VFNAFT_Q4_01	0.006435	ABHD2, CLU, DCLK1, FETUB, GRAF1, GPC4, MB21D2, MYO5A, PPAP2A, PRSS23, RASGRP1, RN144B, THSD4, TPDS2L1
Motif gene sets	YTCF04_05	0.009151	ANKX1, CCR2, CD3G, DPP4, GIMAP6, IL7R, LEF1, RASGRP1, TNFRSF25
Oncogenic signatures	CAMP_UP_V1_DN	1.97E-05	ANKX1, BACE1, CAMK2D, CCR9, CD160, CD83, CHST2, FSTL1, IL7R, NFATC2, TUBB3, ZCCH14
Oncogenic signatures	MEL18_DN_V1_UP	0.03567	CD83, CHST2, CRISPLD2, IL7R, NR2P, NTSE, TEK

Table S2				
Experiment	Study	Significantly detected binding regions	Mapped to genes within 5Kb from TSS	P-value, Significance with WNT-associated genesets from MsigDB
TCF1	GSE52070	591	116	0.033
TCF1 (n=2)	GSE46662	732 in Sample 1	131	0.050
		2600 in Sample 2	653	9.395E-04
TCF7	GSE31221	6395	2015	0.017
Beta-Catenin (n=3)	GSE43565	990 in Sample 1	121	2.273E-04
		385 in Sample 2	49	9.564E-04
		671 in Sample 3	79	0.004

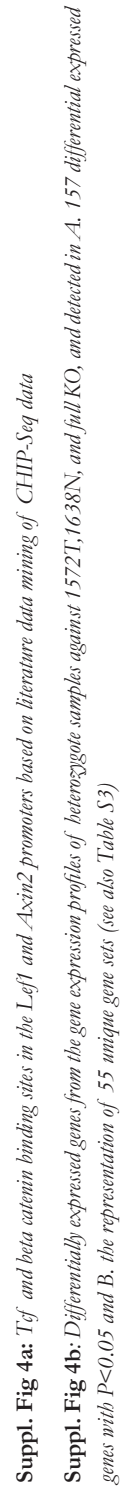


Table S3

Gene-set	Pathway	P _{adj} <0.05	Genes
WNT gene sets	WNT_BOIERS_2013_LYMPHOID	0.01053	CCR9,LEF1,TCF7
All Curated gene sets	ST_WNT_BETA_CATENIN_PATHWAY	0.0001483	APC,AXIN2,DKK2,FSTL1,NKD1,WIF1
All Curated gene sets	RIGGI_EWING_SARCOMA_PROGENITOR_DN	0.0006029	ALDH1A3,BACE1,BMP4,CLU,EBF1,FST,NRP2,PHLDA1,TNFRSF19
All Curated gene sets	SANSOM_WNT_PATHWAY_REQUIRE_MYC	0.001274	AXIN2,LEF1,NKD1,TCF7,TNFRSF19,WIF1
All Curated gene sets	LIU_PROSTATE_CANCER_DN	0.001855	BEND5,CHST2,CLU,EPAS1,ITGA2,NDNF,PHLDA1,PRSS23,ROBO1,TFCP2L1,WIF1,ZCCHC14
All Curated gene sets	MATSUDA_NATURAL_KILLER_DIFFERENTIATION	0.001855	ANXA1,APCDD1,CCR9,CD160,EBF1,NTRK3,PDCD1,PRSS23,SH3BGR2,TCF7,TULP3,ZC3H12C
All Curated gene sets	KINSEY_TARGETS_OF_EWSR1_FLII_FUSION_DN	0.001979	DCLK1,EBF1,FAM63A,FSTL1,IL17RD,MB21D2,NTSE,PHLDA1,PRSS23,SIPA1L2
All Curated gene sets	KUMAR_TARGETS_OF_MLL_AF9_FUSION	0.001979	ANXA1,CCR9,CD83,EBF1,EXTL3,GPC4,IL7R,IRF4,LEF1,TCF7,TNFRSF19
All Curated gene sets	CUI_TCF21_TARGETS_2_UP	0.003067	ANTXR1,APCDD1,ARSB,BMP4,CLU,DCLK1,HUNK,KLF5,LYPD8,NKD1,NRP2
All Curated gene sets	CHARAFE_BREAST_CANCER_LUMINAL_VS_BASAL_DN	0.003672	ADA,ALDH1A3,ANTXR1,ANXA1,FST,FSTL1,IL7R,KLF5,NTSE,PHLDA1,ZC3H12C
All Curated gene sets	DODD_NASOPHARYNGEAL_CARCINOMA_UP	0.003672	ALDH1A3,ANXA1,APCDD1,ATP13A4,BACE1,BDH1,BEND5,CLU,EBF1,EDAR,EPAS1,FAM63A,KLF5,LYPD6B,PRKAA2,PRSS23,SH3BGR2,TNFRSF19,TUBB3,UST,WWC1
All Curated gene sets	DELYS_THYROID_CANCER_UP	0.003672	ALDH1A3,ANXA1,CHST2,DP4,IGSF3,ITGA2,MED13,NRP2,NTSE,PRSS23,STX3
All Curated gene sets	ONDER_CDH1_TARGETS_2_DN	0.004116	ALDH1A3,CD83,EPAS1,FST,IGSF3,ITGA2,KLF5,ROBO1,TFCP2L1,THBD,WWC1
All Curated gene sets	SANA_TNF_SIGNALING_DN	0.004116	ANTXR1,ANXA1,CLU,EPAS1,NTSE,PHLDA1
All Curated gene sets	KEGG_WNT_SIGNALING_PATHWAY	0.004871	APC,AXIN2,DKK2,LEF1,NKD1,TCF7,WIF1
All Curated gene sets	KEGG_BASAL_CELL_CARCINOMA	0.005932	APC,AXIN2,BMP4,LEF1,TCF7
All Curated gene sets	CUI_TCF21_TARGETS_2_DN	0.006368	ANXA1,ARHGAP28,BACE1,DKK2,DP4,EBF1,EPAS1,MED13,NTSE,PPAP2A,SH3BGR2,SHROOM3,SNCAIP,THBD
All Curated gene sets	BYSTRYKH_HEMATOPOIESIS_STEM_CELL_QTL_TRANS	0.01287	AXIN2,CHST2,EHFD1,EXTL3,FAM63A,GPC4,KIF5C,LEF1,PDCL1,STX3,SULT1A1,TFCP2L1,THBD,TULP3
All Curated gene sets	GAUSSMANN_MLL_AF4_FUSION_TARGETS_F_UP	0.0141	ARHGAP28,ARSB,BMP4,FST,GPC4,IL17RD,NTSE
All Curated gene sets	CHARAFE_BREAST_CANCER_LUMINAL_VS_MESENCHYMAL_DN	0.01879	ANTXR1,ANXA1,CHST2,FST,FSTL1,IL7R,NTSE,PHLDA1,RAI14,ZC3H12C
All Curated gene sets	GOZGIT_ESR1_TARGETS_DN	0.03962	CLU,DCLK1,FETUB,GPC4,MB21D2,PPAP2A,PRSS23,RASGRP1,SH3BGR2,SHROOM3,SIPA1L2,THBD
All Curated gene sets	ENK_UV_RESPONSE_EPIDERMIS_DN	0.04184	ANXA1,APC,CD83,ITGA2,PHLDA1,PPAP2A,PRSS23,RAI14,ROBO1,THBD
All Curated gene sets	WNT_SIGNALING	0.04194	APC,LEF1,NKD1,TCF7,WIF1
All Curated gene sets	PID_P1_PATHWAY	0.04605	APC,DKK2,NKD1,WIF1
All Curated gene sets	SENESE_HDAC1_AND_HDAC2_TARGETS_UP	0.04605	DCLK1,DKK2,EXTL3,IL7R,NRIP3,PHLDA1,WWC1
All Curated gene sets	KIM_MYC_AMPLIFICATION_TARGETS_DN	0.04605	ANXA1,APC,AXIN2,BDH1,BMP4,CCDC109B,CD83,EBF1,EDAR,EXTL3,FAM63A,FST,FSTL1,IL7R,IRF4,ITGA2,KCNIP2,KLF5,NKD1,NRP2,NTRK3,RNF214,ROBO1,SNCAIP,TNFRSF19,XKRX,ZCCHC14
Motif gene sets	TTGTTT_V\$FOXO4_01	3.15E-05	ATP13A4,BACE1,CD160,CPB1,FAM63A,FST,GPC4,KY,LEF1,MB21D2,MED13,NKD1,NRP2,ROBO1,SLC22A23,SNCAIP,TCF7,TNFRSF19,XKRX
Motif gene sets	CTTTGA_V\$LEF1_Q2	0.0003071	ACTN2,AXIN2,BACE1,BMP4,CD83,CPB1,EBF1,EDAR,EPAS1,EXTL3,FST,IGSF3,ITGA2,KCNIP2,LEF1,LYPD6B,MB21D2,NRIP3,NRP2,NTRK3,SH3BGR2,SNCAIP,TCF7,UNC45B,UST,WWC1
Motif gene sets	CAGGTG_V\$E12_Q6	0.001973	FAM63A,FST,GPC4,KY,NKD1,NRP2,TCF7,TNFRSF19
Motif gene sets	V\$TCF4_Q5	0.005048	ANTXR1,BMP4,DCLK1,DKK2,EBF1,EHFD1,FST,FSTL1,IGSF3,IL17RB,IL7R,IRF4,ITGA2,KCNIP2,KLF5,MED13,SH3BGR2,SNCAIP,TMEM163,TNFRSF19,XKRX
Motif gene sets	TGGA AAA_V\$NFAT_Q4_01	0.006748	ARHGAP28,BACE1,CHST2,EDAR,MED13,RNF214,UST,ZCCHC14
Motif gene sets	TATTATA_MIR-374	0.01408	AHSG,AXIN2,DCLK1,KY,LEF1,MB21D2,MED13,NRP2,NTRK3,RAI14,ROBO1,XKRX
Motif gene sets	TGCCAAR_V\$NF1_Q6	0.01468	AXIN2,BMP4,FST,FSTL1,IRF4,KY,NTRK3,ROBO1,SNCAIP,TCF7,TNFRSF19,UNC45B,UST
Motif gene sets	RTAAACA_V\$FREAC2_01	0.02911	ANXA1,BACE1,CCR9,CD160,CD83,CHST2,FSTL1,IL7R,TUBB3,ZCCHC14
Oncogenic signatures	CAMP_UP.V1_DN	5.78E-06	AXIN2,EDARADD,TNFRSF19,TULP3,WIF1,ZC3H12C
Oncogenic signatures	AKT_UP.V1_DN	0.04519	ADA,AXIN2,CCDC109B,DP4,EDARADD,IL17RB,IL7R,PDCD1,TUBB3
Immunologic signatures	GSE24142_EARLY_THYMIC_PROGENITOR_VS_DN2_THYMOCYTE_DN	0.001121	ACTN2,CD160,EPAS1,GPR114,IL17RB,RASGRP1,THBD,XKRX
Immunologic signatures	GSE20366_EX_VIVO_VS_DEC205_CONVERSION_NAIVE_CD4_TCELL_UP	0.007534	ANXA1,CCDC109B,DP4,IL7R,LEF1,TCF7,ZCCHC14
Immunologic signatures	GSE10325_LUPUS_CD4_TCELL_VS_LUPUS_BCELL_UP	0.01556	CCDC109B,CD160,CD83,KY,NTSE,PDCD1,ZC3H12C
Immunologic signatures	GSE14350_IL2RB_KO_VS_WT_TREG_DN	0.01556	ADA,CCDC109B,IL7R,LEF1,PDCD1,TUBB3,TULP3
Immunologic signatures	GSE24142_EARLY_THYMIC_PROGENITOR_VS_DN3_THYMOCYTE_DN	0.01556	AXIN2,CCDC109B,EDARADD,IL17RB,IL7R,LEF1,PPAP2A
Immunologic signatures	GSE24142_EARLY_THYMIC_PROGENITOR_VS_DN2_THYMOCYTE_ADULT_DN	0.01556	BDH1,BEND5,EDAR,EHFD1,LEF1,NTSE,PPAP2A
Immunologic signatures	GSE26495_NAIVE_VS_PD1HIGH_CD8_TCELL_UP	0.01556	BDH1,BEND5,EDAR,EHFD1,LEF1,NTSE,PPAP2A
Immunologic signatures	GSE26495_NAIVE_VS_PD1LOW_CD8_TCELL_UP	0.01556	AHSG,ANXA1,EPAS1,GPR114,PRKAA2,RASGRP1,TMEM163
Immunologic signatures	GSE30962_PRIMARY_VS_SECONDARY_CHRONIC_LCMV_INF_CD8_TCELL_DN	0.01556	DP4,IL7R,ITGA2,NDNF,PHLDA1,PRKAA2,TCF7
Immunologic signatures	GSE3982_BCELL_VS_CENT_MEMORY_CD4_TCELL_DN	0.01556	CD83,DP4,IRF4,NTSE,PPAP2A,SH3BGR2,ZC3H12C
Immunologic signatures	GSE7460_TCONV_VS_TREG_LN_DN	0.01556	CCDC109B,CD83,IGSF3,KIF5C,NRP2,PPAP2A,SH3BGR2
Immunologic signatures	GSE7460_TCONV_VS_TREG_THYMUS_DN	0.01556	CCDC109B,CD83,IGSF3,KIF5C,PDCD1,PPAP2A,SH3BGR2
Immunologic signatures	GSE7852_TREG_VS_TCONV_THYMUS_UP	0.01556	AXIN2,LEF1,NKD1,TCF7
Hallmark gene sets	HALLMARK_WNT_BETA_CATENIN_SIGNALING	0.002609	ANXA1,CLU,DP4,ITGA2,PRSS23,THBD
Hallmark gene sets	HALLMARK_COAGULATION	0.002609	CD83,IRF4,NTSE,PHLDA1,PPAP2A,SH3BGR2
Hallmark gene sets	HALLMARK_IL2_STATS_SIGNALING	0.007102	CHST2,CPB1,EDAR,EHFD1,PDCD1,TFCP2L1
Hallmark gene sets	HALLMARK_KRAS_SIGNALING_DN	0.007102	FAM63A,IL17RB,PRSS23,RASGRP1,WWC1
Hallmark gene sets	HALLMARK_ESTROGEN_RESPONSE_EARLY	0.04111	ACTN2,CLU,DP4,KCNIP2,RASGRP1
Hallmark gene sets	HALLMARK_COMPLEMENT	0.04111	

References

1. Blank U., Karlsson G., Karlsson S. Signaling pathways governing stem-cell fate. *Blood*. 2008;111:492–503.
2. Duinhouwer L.E., Tuysuz N., Rombouts E.W., Ter Borg M.N., Mastrobattista E., Spanholtz J., Cornelissen J.J., Ten Berge D., Braakman E. Wnt3a protein reduces growth factor-driven expansion of human hematopoietic stem and progenitor cells in serum-free cultures. *PLoS One*. 2015;10:e0119086.
3. Famili F., Naber B.A., Vloemans S., De Haas E.F., Tiemessen M.M., Staal F.J. Discrete roles of canonical and non-canonical Wnt signaling in hematopoiesis and lymphopoiesis. *Cell Death Dis*. 2015;6:e1981.
4. Fleming H.E., Janzen V., Lo Celso C., Guo J., Leahy K.M., Kronenberg H.M., Scadden D.T. Wnt signaling in the niche enforces hematopoietic stem cell quiescence and is necessary to preserve self-renewal in vivo. *Cell Stem Cell*. 2008;2:274–283.
5. Gaspar C., Fodde R. APC dosage effects in tumorigenesis and stem cell differentiation. *Int. J. Dev. Biol*. 2004;48:377–386.
6. Goessling W., North T.E., Loewer S., Lord A.M., Lee S., Stoick-Cooper C.L., Weidinger G., Puder M., Daley G.Q., Moon R.T. Genetic interaction of PGE2 and Wnt signaling regulates developmental specification of stem cells and regeneration. *Cell*. 2009;136:1136–1147.
7. Harada N., Tamai Y., Ishikawa T., Sauer B., Takaku K., Oshima M., Taketo M.M. Intestinal polyposis in mice with a dominant stable mutation of the beta-catenin gene. *EMBO J*. 1999;18:5931–5942.
8. Huang J., Zhang Y., Bersenev A., O'Brien W.T., Tong W., Emerson S.G., Klein P.S. Pivotal role for glycogen synthase kinase-3 in hematopoietic stem cell homeostasis in mice. *J. Clin. Invest*. 2009;119:3519–3529.
9. Huang J., Nguyen-McCarty M., Hexner E.O., Danet-Desnoyers G., Klein P.S. Maintenance of hematopoietic stem cells through regulation of Wnt and mTOR pathways. *Nat. Med*. 2012;18:1778–1785.
10. Jeannet G., Scheller M., Scarpellino L., Duboux S., Gardiol N., Back J., Kuttler F., Malanchi I., Birchmeier W., Leutz A. Long-term, multilineage hematopoiesis occurs in the combined absence of beta-catenin and gamma-catenin. *Blood*. 2008;111:142–149.
11. Kabiri Z., Numata A., Kawasaki A., Edison, Tenen D.G., Virshup D.M. Wnts are dispensable for differentiation and self-renewal of adult murine hematopoietic stem cells. *Blood*. 2015;126:1086–1094.
12. Kirstetter P., Anderson K., Porse B.T., Jacobsen S.E., Nerlov C. Activation of the canonical Wnt pathway leads to loss of hematopoietic stem cell repopulation and multilineage differentiation block. *Nat. Immunol*. 2006;7:1048–1056.
13. Koch U., Wilson A., Cobas M., Kemler R., Macdonald H.R., Radtke F. Simultaneous loss of β - and γ -catenin does not perturb hematopoiesis or lymphopoiesis. *Blood*. 2008;111:160–164.
14. Lane S.W., Sykes S.M., Al-Shahrour F., Shterental S., Paktinat M., Lo Celso C., Jesneck J.L., Ebert B.L., Williams D.A., Gilliland D.G. The *Apc(min)* mouse has altered hematopoietic stem cell function and provides a model for MPD/MDS. *Blood*. 2010;115:3489–3497.
15. Lane S.W., Wang Y.J., Lo Celso C., Ragu C., Bullinger L., Sykes S.M., Ferraro F., Shterental S., Lin C.P., Gilliland D.G. Differential niche and Wnt requirements during acute myeloid leukemia progression. *Blood*. 2011;118:2849–2856.
16. Li W., Hou Y., Ming M., Yu L., Seba A., Qian Z. *Apc* regulates the function of hematopoietic stem cells largely through beta-catenin-dependent mechanisms. *Blood*. 2013;121:4063–4072.
17. Luis T.C., Weerkamp F., Naber B.A., Baert M.R., de Haas E.F., Nikolic T., Heuvelmans S., De Krijger R.R., van Dongen J.J., Staal F.J. Wnt3a deficiency irreversibly impairs hematopoietic stem cell self-renewal and leads to defects in progenitor cell differentiation. *Blood*. 2009;113:546–554.

18. Luis T.C., Naber B.A., Roozen P.P., Brugman M.H., de Haas E.F., Ghazvini M., Fibbe W.E., van Dongen J.J., Fodde R., Staal F.J. Canonical wnt signaling regulates hematopoiesis in a dosage-dependent fashion. *Cell Stem Cell*. 2011;9:345–356.
19. Luis T.C., Ichii M., Brugman M.H., Kincade P., Staal F.J. Wnt signaling strength regulates normal hematopoiesis and its deregulation is involved in leukemia development. *Leukemia*. 2012;26:414–421.
20. Malhotra S., Kincade P.W. Wnt-related molecules and signaling pathway equilibrium in hematopoiesis. *Cell Stem Cell*. 2009;4:27–36.
21. Mendez-Ferrer S., Michurina T.V., Ferraro F., Mazloom A.R., Macarthur B.D., Lira S.A., Scadden D.T., Ma'ayan A., Enikolopov G.N., Frenette P.S. Mesenchymal and haematopoietic stem cells form a unique bone marrow niche. *Nature*. 2010;466:829–834.
22. Ming M., Wang S., Wu W., Senyuk V., Le Beau M.M., Nucifora G., Qian Z. Activation of Wnt/beta-catenin protein signaling induces mitochondria-mediated apoptosis in hematopoietic progenitor cells. *J. Biol. Chem*. 2012;287:22683–22690.
23. Oostendorp R.A. Secretion of Wnts is dispensable for hematopoiesis. *Blood*. 2015;126:1051–1052.
24. Perry J.M., He X.C., Sugimura R., Grindley J.C., Haug J.S., Ding S., Li L. Cooperation between both Wnt/{beta}-catenin and PTEN/PI3K/Akt signaling promotes primitive hematopoietic stem cell self-renewal and expansion. *Genes Dev*. 2011;25:1928–1942.
25. Reya T., Clevers H. Wnt signalling in stem cells and cancer. *Nature*. 2005;434:843–850.
26. Reya T., Duncan A.W., Ailles L., Domen J., Scherer D.C., Willert K., Hintz L., Nusse R., Weissman I.L. A role for Wnt signalling in self-renewal of haematopoietic stem cells. *Nature*. 2003;423:409–414.
27. Scheller M., Huelsken J., Rosenbauer F., Taketo M.M., Birchmeier W., Tenen D.G., Leutz A. Hematopoietic stem cell and multilineage defects generated by constitutive beta-catenin activation. *Nat. Immunol*. 2006;7:1037–1047.
28. Smits R., Kielman M.F., Breukel C., Zurcher C., Neufeld K., Jagmohan-Changur S., Hofland N., van Dijk J., White R., Edelmann W. Apc1638T: a mouse model delineating critical domains of the adenomatous polyposis coli protein involved in tumorigenesis and development. *Genes Dev*. 1999;13:1309–1321.
29. Smits R., Hofland N., Edelmann W., Geugien M., Jagmohan-Changur S., Albuquerque C., Breukel C., Kucherlapati R., Kielman M.F., Fodde R. Somatic Apc mutations are selected upon their capacity to inactivate the beta-catenin downregulating activity. *Genes Chromosomes Cancer*. 2000;29:229–239.
30. Staal F.J., Luis T.C., Tiemessen M.M. WNT signalling in the immune system: WNT is spreading its wings. *Nat. Rev. Immunol*. 2008;8:581–593.
31. van Es J.H., Jay P., Gregorieff A., van Gijn M.E., Jonkheer S., Hatzis P., Thiele A., van den Born M., Begthel H., Brabletz T. Wnt signalling induces maturation of Paneth cells in intestinal crypts. *Nat. Cell Biol*. 2005;7:381–386.
32. Wang Y., Krivtsov A.V., Sinha A.U., North T.E., Goessling W., Feng Z., Zon L.I., Armstrong S.A. The Wnt/beta-catenin pathway is required for the development of leukemia stem cells in AML. *Science*. 2010;327:1650–1653.
33. Zhao C., Blum J., Chen A., Kwon H.Y., Jung S.H., Cook J.M., Lagoo A., Reya T. Loss of beta-catenin impairs the renewal of normal and CML stem cells in vivo. *Cancer Cell*. 2007;12:528–541.

